ACS OMEGA

Open Access

http://pubs.acs.org/journal/acsodf

Article

Drug-Loaded Polycaprolactone/Fibroin/Polydopamine Composite Coating on an Anodized Titanium Surface with Calcium and Phosphorus Deposited Using Electrospray Technology

Hao An, Yu-Kyoung Kim,* Yong-Seok Jang,* and Min-Ho Lee*

Cite This: *ACS Omega* 2025, 10, 14593−14601

Read Online

ACCESS | Metrics & More | Article Recommendations

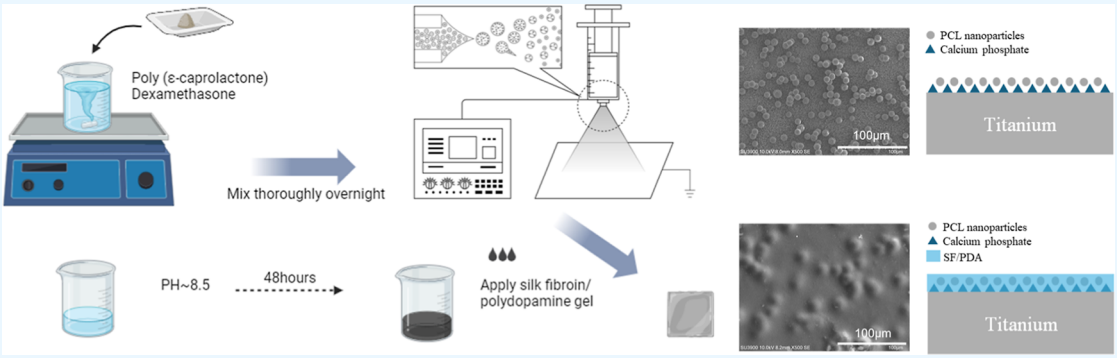

ABSTRACT: Due to the low bioactivity of titanium implants, the extended bone integration process after implantation substantially heightens the risk of inflammation, a primary cause of implant failure. To mitigate inflammatory responses and enhance bone integration between the implant and bone tissue, based on prior research that applied calcium phosphate (CaP) on titanium surfaces, we employed electrospraying technology to develop a drug-loaded polycaprolactone/silk fibroin/polydopamine (PCL/SF/PDA) composite coating as the second layer on top of the calcium phosphate deposition. The surface morphologies of the CaP deposits and composite coatings were characterized by SEM. The SF/PDA gel significantly increased the adhesion of the coating, thereby enhancing its clinical application potential. All materials exhibited excellent biodegradability, and their superior biocompatibility was confirmed through cell assays. Following in vitro experiments, in vivo studies were conducted using a rat cranial defect model. Micro-CT results and staining demonstrated that CaP deposition significantly accelerated bone integration between the titanium substrate and bone, while the drug-loaded polymer coating notably improved the inflammatory environment at the defect site. These findings offer new insights into the development of titanium implants.

INTRODUCTION

Titanium (Ti) implants have been extensively researched due to their excellent mechanical properties, biocompatibility, and corrosion resistance.[1−3] Despite their high biocompatibility, the inherently bioinert nature of Ti results in relatively low bioactivity, often requiring several months for complete bone integration.[4−7] To enhance the bioactivity of Ti, additional surface treatments that control inflammation and accelerate bone formation are strongly recommended. These treatments ensure that Ti, as an exceptional implant material, fully maximizes its potential in the bone integration process.

Enhancing the surface activity of Ti implants and mitigating the inflammatory environment are of paramount importance for improving the repair effects of implants. This challenge is the primary focus of the present study. Previous studies have demonstrated the successful deposition of micrometer-level calcium phosphate (CaP) on a Ti surface through anodization and calcium cycling, significantly enhancing the bone integration capability of the Ti surface.[8,9] However, the issue of inflammation has not yet been effectively addressed. Biodegradable polymer coatings are a promising surface modification technology as most polymer materials are highly biocompatible[10] and can reduce foreign body reactions and chronic inflammation. By embedding drugs into polymers,[11] such as polylactic acid, polyglycolic acid, and polylactic-*co*-glycolic acid, a slow release of drugs can be achieved,

Received: July 22, 2024
Revised: February 6, 2025
Accepted: April 2, 2025
Published: April 10, 2025

promoting the healing process and reducing the inflammatory environment.

In this study, we used dexamethasone, a synthetic corticosteroid with excellent anti-inflammatory and immunosuppressive properties.[12] Dexamethasone controls inflammation in postsurgical bone defect areas by inhibiting the production of inflammatory mediators, reducing the migration and activity of inflammatory cells, and decreasing tissue reactivity. Polycaprolactone (PCL) is a highly biocompatible and biodegradable material with remarkable permeability to various drugs[11,13−15] and has been widely used in the fabrication of drug delivery systems and scaffolds. Electrospraying is an innovative droplet ejection technique[16−19] in which a charged liquid sample is ejected from the tip of a needle under a strong electric field and continuously torn by the electric field to form tiny droplets during spraying. These tiny droplets dry rapidly in the air and eventually form uniform nanoparticles that cover the substrate surface. This method can precisely control the morphology and size of polymer particles, ensuring uniform particle distribution, near monodispersity, high drug encapsulation efficiency, and minimal adverse effects on active ingredients (e.g., denaturation) during the process.[19−22] Additionally, the nanoparticle coating produced by electrospray has high uniformity, effectively addressing many disadvantages of traditional dip-coating methods, such as uneven coating, low drug loading rate, and uncontrollable thickness,[23,24] which can greatly improve the biocompatibility of the drug-loaded coating.

To address the issue of coating detachment in clinical applications, silk fibroin (SF) and polydopamine (PDA), two innovative materials with excellent adhesiveness, were introduced. Both are degradable materials with exceptional biocompatibility.[25,26] SF, a key component of silkworm cocoons, is rich in amino acids such as glycine, serine, and proline. It exhibits both hydrophilic and hydrophobic properties, enhancing its ability to adhere to and adsorb onto various surfaces.[27,28] Dopamine (DA) was also applied to increase the adhesion of the coating layer. The remarkable adhesion of mussels is primarily attributed to the secretion of mucin, which is rich in 3,4-dihydroxy-L-phenylalanine, commonly known as DA.[29−31] This characteristic enables PDA to readily form bonds with various metal surfaces. Studies have shown that the amino group of SF binds to the quinone structure of oxidized DA via a Schiff base reaction. Subsequently, free dopamine forms a SF/dopamine (SF/PDA) complex hydrogel through the self-polymerization of dopamine bound to SF,[25,32] exhibiting a strong adhesive effect. Therefore, SF/PDA gel was applied to the PCL nanoparticle coating using a dip-coating method; a PCL/SF/PDA composite coating was prepared on top of the CaP deposition as a second layer.

We described the application of electrospraying to create a biodegradable, drug-loaded coating on the surface of a CaP-deposited Ti plate. Dexamethasone, a potent anti-inflammatory drug, was chosen to mitigate inflammatory responses at the implantation site. The morphology, drug release profile, and degradation characteristics of the drug-loaded coating were evaluated through material characterization techniques. The adhesion properties of the composite coating were analyzed to determine its suitability for clinical implantation. Additionally, its biocompatibility and bone integration capabilities were assessed through both in vitro and in vivo studies.

MATERIALS AND METHODS

Materials. Polycaprolactone (Mn 80,000) was utilized for nanoparticle synthesis, while dichloromethane (MW 84.93) served as the solvent for electrospraying. Dexamethasone (MW 392.46) was incorporated for drug loading. SF (MW 100 kDa) and dopamine hydrochloride (MW 189.64) were procured from Sigma-Aldrich (St. Louis, MO, USA).

Preparation of CaP Coating and Composite Coating. CaP deposition was conducted using an electrochemical anodization method based on previous studies.[9,33−35] A Ti plate (1 cm × 1 cm) was immersed in a pickling solution (HNO_3 and HF) for degreasing. Anodization was performed with a glycerine-based electrolyte containing 1 wt % NH_4F. The two-electrode system involved connecting the Ti sample and a platinum plate to the anode and cathode, respectively, of a power supply (SPD 303D, Daininotek, South Korea). A voltage of 20 V was maintained for 1 h. The anodized samples were rinsed with 0.5 vol % $NaSiO_3$ and dried at room temperature. Subsequently, the samples were subjected to precalcification by immersing them in 0.05 M NaH_2PO_4 (80 °C, 1 min) and saturated $Ca(OH)_2$ (90 °C, 1 min) for 20 cycles. The samples were then annealed at 500 °C for 2 h (with a heating rate of 10 °C per minute) to stabilize the crystal structure.

SF particles were completely dissolved in distilled water at a concentration of 50 mg/mL (pH 8.5). DA powder (2 mg) was dissolved in 1 mL of the SF solution, thoroughly stirred in a dark environment to avoid air exposure, and incubated at 37 °C for 72 h for DA oxidation.[25,32] The electrospray was based on previous research, with some adjustments made to the method.[36] PCL and dexamethasone were dissolved in dichloromethane to obtain a 3.5 wt % PCL drug carrier solution, mixed thoroughly overnight to ensure uniformity. The solution was loaded into an electrospray machine with a syringe diameter of 15.89 mm, and a spraying rate of 35 μL/min was maintained. A CaP-coated Ti sheet was placed at the center of the collector. The needle and collector were connected to the anode and cathode of a high-voltage direct current (HVDC) power supply at a fixed vertical distance of 150 mm. The sample was immersed in the SF/PDA gel using the dipping method postelectrospray process. Finally, the PCL/SF/PDA composite coating was obtained by drying the sample in an incubator at 37 °C for 2 h.

Characterization of Composite Coating and Nanoparticles. The morphology of the nanoparticles and composite coating was examined using scanning electron microscopy (SEM; SU-70, Hitachi, Tokyo, Japan). PCL particle size in the SEM results was analyzed using ImageJ software (National Institutes of Health, Bethesda, MD, USA). Fourier transform infrared spectroscopy (FT-IR) (Spectrum RX1 FT-IR spectrometer, PerkinElmer) was employed to measure the absorbance of the samples across the frequency range of 4000−400 cm^{-1}. The adhesive properties of the composite coatings were evaluated via tape tests and the surface morphology of the samples was observed using microscopy (DM 2500M; Leica, Germany). Samples coated with the PCL/SF/PDA composite coating, size (1 cm × 1 cm), were placed in 15 mL conical tubes and immersed completely in 5 mL of phosphate-buffered saline (PBS). The tubes were incubated in a incubator at 37 °C. The samples were taken out for drying at various points in time, and the morphology was observed by SEM to assess the degradation of the coatings. For

https://doi.org/10.1021/acsomega.4c06731
ACS Omega 2025, 10, 14593−14601

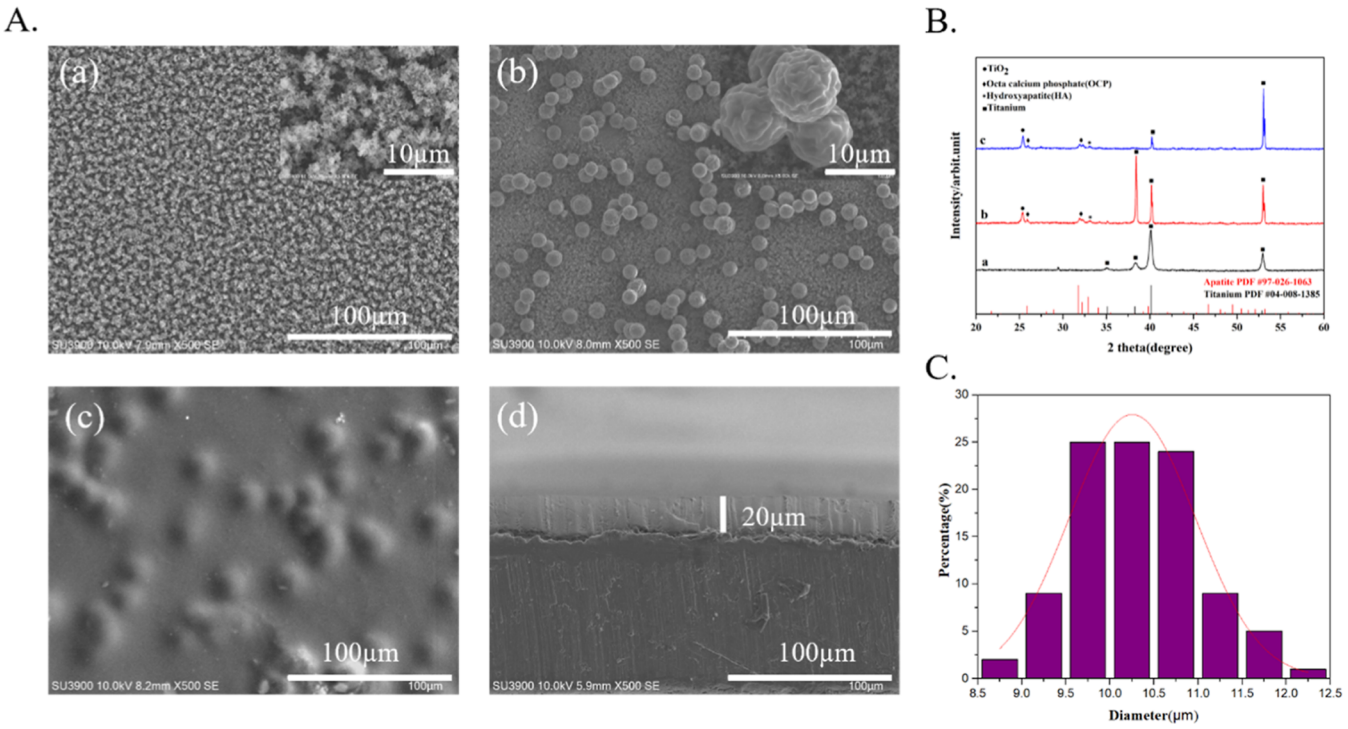

Figure 1. Characterization of composite coatings. (A) Scanning electron microscopy (SEM) images showing (a) calcium phosphate/titanium (CaP/Ti), (b) calcium phosphate/titanium loaded with polycaprolactone nanoparticles(CaP/Ti/PCL), (c) calcium phosphate/titanium/polycaprolactone coated with silk fibroin/polydopamine coating (CaP/Ti/PCL/SF/PDA), and (d) cross-section of CaP/Ti/PCL/SF/PDA. (B) X-ray diffraction (XRD) patterns of (a) titanium, (b) CaP/Ti, and (c) CaP/Ti/PCL/SF/PDA. (C) Polycaprolactone (PCL) nanoparticle size analysis.

drug release detection, the samples, size (1 cm × 1 cm), were placed in 15 mL conical tubes and they were completely immersed in 10 mL phosphate-buffered saline (PBS), and the absorbance at 240 nm was measured by UV−vis spectroscopy (Scinco, Seoul, South Korea) 15 min, 30 min, 1 h, 2 h, 4 h, 8 h, 12 h, and 24 h later.

In Vitro Studies. The cell culture medium was formulated by supplementing α-minimal essential medium (α-MEM, Gibco, Carlsbad, CA, USA) with 10% fetal bovine serum (FBS, Gibco Co., USA), 500 U/mL streptomycin, and penicillin (both from Gibco, Grand Island, NY, USA). Sample extracts were prepared according to ISO 10993-12. MC3T3-E1 cells (2×10^4 cells/24 well, ATCC, American Type Culture Collection) were incubated with the extracts. Cells grown without the extract served as the control group. After 2 and 5 days of culture, cell proliferation was assessed using a CCK-8 kit (Enzo Life Sciences Inc., New York, NY, USA). The cells were stained with crystal violet for observation.

In Vivo Studies. Sixteen male Sprague−Dawley rats (270−280 g; Damul Science, Daejeon, Korea) were used in this experiment. All animal experiments were performed in accordance with the National Research Council's Guide for the Care and Use of Laboratory Animals and approved by the Laboratory Animal Center at Jeonbuk National University in Jeonju-si, South Korea (approval number: NON2023-206-001). To create a calvarial defect, rats were anesthetized using a combination of Zoletil (Zoletil 50, Virbac Laboratories, France) and xylazine hydrochloride (Rompun; Bayer Korea Ltd., Republic of Korea). A surgical trephine was used to create two symmetrical circular defects with diameters of 5 mm on the calvarium. A circular Ti sheet with a diameter of 5.5 mm was prepared, and the Ca−P layer was deposited onto the Ti surface following the method described above. Subsequently, a PCL/SF/PDA composite coating was applied using a combination of electrospray and dip-coating techniques. Various groups were compared, including the defect, pure Ti, CaP/Ti, and CaP/Ti/PCL/SF/PDA groups. The rats were euthanized with an overdose of isoflurane (Hana Pharma Corporation, Seoul, South Korea), and the collected tissues were analyzed using micro-CT (SKYSCAN 1076, Skyscan, Belgium). Histological analysis was performed on three animals from each group at 2- and 4 weeks postsurgery. Skull pieces were stained with Villanueva solution (Polysciences, Inc., USA) and embedded in poly(methyl methacrylate). The resin blocks containing the samples were cut vertically along the plane of the Ti film through the central point. The polished slices were observed under an optical microscope (DM 2500M; Leica, Germany).

Statistical Analysis. To assess statistical significance, one-way analysis of variance (ANOVA) was conducted with a 95% confidence interval. Analyses were performed using GraphPad Prism version 8.0.2 (GraphPad Software, La Jolla, CA, USA). A p-value of less than 0.05 was considered significant.

RESULTS

A microsized CaP deposition layer was formed on the Ti surface through anodization and cyclic precalcification. As shown in Figure 1B, X-ray diffraction (XRD) data indicate the presence of octacalcium phosphate (OCP) and hydroxyapatite (HA) in the CaP samples. The solution was expelled from the nozzle under the influence of a strong electric field after connecting the positive and negative terminals of a high-voltage direct current power supply. Figure 1A(a and b) shows SEM images of the CaP/Ti surface before and after the

https://doi.org/10.1021/acsomega.4c06731
ACS Omega 2025, 10, 14593−14601

electrospraying of PCL nanoparticles. Following this preparation, the Ti surface with the CaP deposit was uniformly covered with PCL nanoparticles by electrospraying, exhibiting a uniform distribution and particle size. ImageJ analysis, shown in Figure 1C, indicates that the average particle size of these nanoparticles was approximately 10.25 μm, with the particle size being uniform and controllable. Figure 1A(c and d) shows that the SF/PDA hydrogel successfully encapsulated the PCL nanoparticles and filled the gaps between them, forming a PCL/SF/PDA composite coating on the CaP-coated Ti surface. The thickness of this composite coating is approximately 20 μm.

As depicted in Figure 2a, characteristic peaks of DA were identified at 3336.73 cm^{-1}, 3036.77 cm^{-1}, 2956.15 cm^{-1}, and 1498.08 cm^{-1}. Upon treatment in a weakly alkaline environment, these distinct peaks disappeared, as illustrated in Figure 2b, and new, weaker peaks emerged within the range of 3500−2800 cm^{-1}, indicating the stretching vibrations of free $-NH_2$ groups in PDA. This self-polymerization process was effectively achieved in a mildly alkaline environment at pH 8.5. Additionally, Figure 2c displayed absorption peaks at 1638.85 cm^{-1}, 1513.63 cm^{-1}, and 1233.83 cm^{-1} attributed to the vibrations of the amide I, amide II, and amide III bands in SF, respectively, along with a peak at 3279.26 cm^{-1} corresponding to the vibration of hydroxyl groups in SF. In Figure 2e, peaks located at 1093.60 cm^{-1}, 1028.01 cm^{-1}, 964.11 cm^{-1}, 601.20 cm^{-1}, and 562.54 cm^{-1} were identified as belonging to PO_4^{2-} groups in CaP. Following coating with PCL nanoparticles, all PO_4^{2-} peaks were obscured, replaced by peaks characteristic of PCL at 2943.88 cm^{-1} for asymmetric $-CH_2$ stretching, 2866.20 cm^{-1} for symmetric $-CH_2$ stretching, 1722.91 cm^{-1} for carbonyl stretching, 1294.02 cm^{-1} for C−O and C−C stretching, 1239.96 cm^{-1} for asymmetric C−O−C stretching, and 1163.51 cm^{-1} for symmetric C−O−C stretching. In the CaP/Ti/PCL/SF/PDA group, due to the shielding effect of the SF/PDA hydrogel, only peaks located at 3268.11 cm^{-1}, 1638.45 cm^{-1}, 1515.02 cm^{-1}, and 1236.38 cm^{-1} corresponding to SF were detected. Although no additional peaks were observed in the SF/PDA hydrogel, all peaks were notably intensified following the incorporation of PDA, indicating increased hydrogen bonding within the SF/PDA hydrogel.

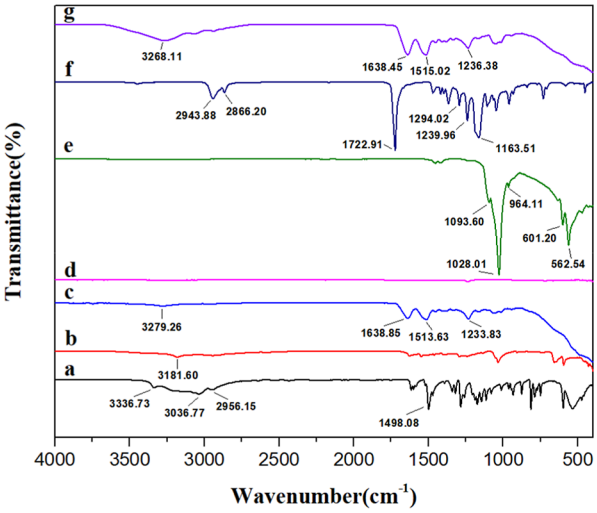

Figure 2. FT-IR spectra of materials. FT-IR spectra of (a) dopamine (DA), (b) polydopamine (PDA), (c) silk fibroin (SF), (d) titanium (Ti), (e) CaP/Ti, (f) CaP/Ti/PCL, and (g) CaP/Ti/PCL/SF/PDA.

A tape test was conducted to assess the adhesive properties of the coatings in Figure 3, with microscopic examination performed before and after testing. In the PCL group, the coating exhibited a loose structure, resulting in significant detachment of PCL nanoparticles upon tape application and removal. Conversely, the PCL/SF/PDA group demonstrated superior adhesion, with minimal dislodgement of PCL nanoparticles.

To evaluate the degradation behavior of the composite coatings, samples were immersed in PBS and subsequently analyzed using SEM. As depicted in Figure 4, the outer layer of the SF/PDA hydrogel began degrading within 24 h, gradually exposing the internal drug-loaded PCL nanoparticles. Additionally, Figure 5 illustrates the release of dexamethasone into the solution, quantified via UV−visible spectroscopy within the

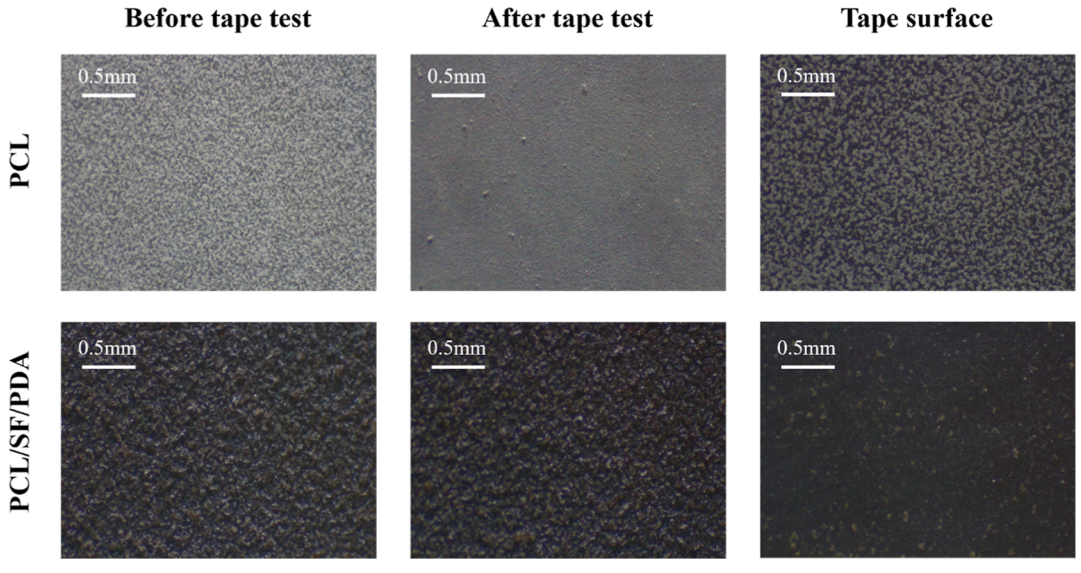

Figure 3. Adhesion assessment by the tape test.

https://doi.org/10.1021/acsomega.4c06731
ACS Omega 2025, 10, 14593−14601

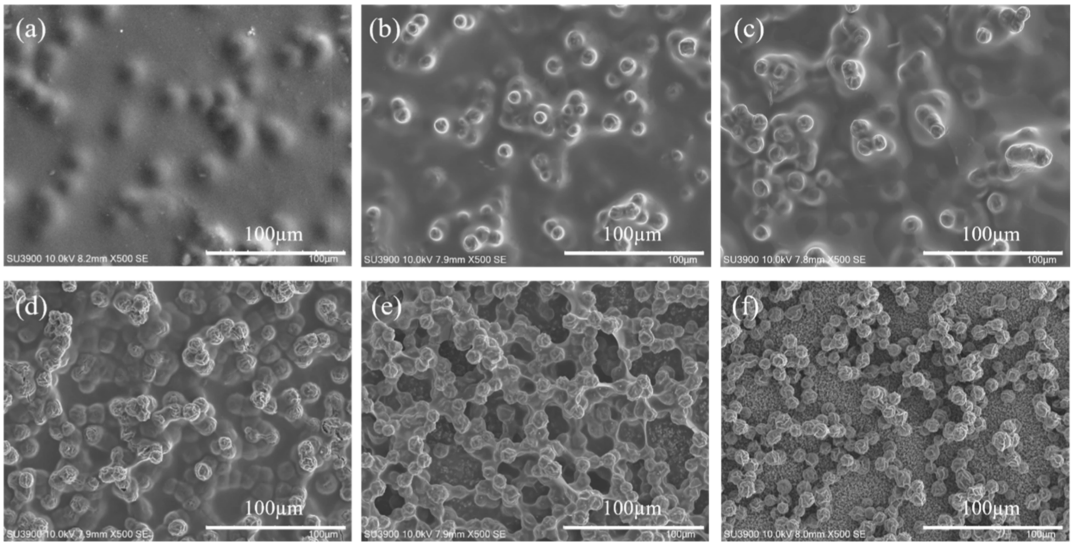

Figure 4. SEM images of degradation of composite coating. SEM images of the CaP/Ti/PCL/SF/PDA composite coating after (a) deposition and degradation at various time intervals: (b) 15 min, (c) 30 min, (d) 1 h, (e) 2 h, and (f) 24 h.

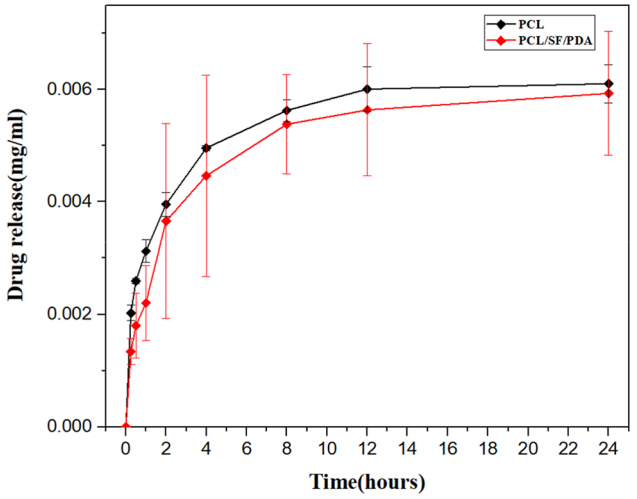

Figure 5. Drug release curves within 24 h.

same time frame. Initially, the drug release rate from the composite coating was significantly slower compared to that of the pure PCL coating, attributed to the protective effect of the SF/PDA layer. However, after 24 h, the release rates between the two groups converged, indicating a reduction in the barrier effect of the SF/PDA hydrogel over time.

Figure 6 depicts osteoblast proliferation evaluated via the CCK-8 assay after 2 and 5 days of cell culture. The results indicated no statistically significant differences in optical density (OD) values among the three groups. Each experimental group exhibited cell viability exceeding 90% compared to the control group. Notably, after 2 days, the OD value of the sample group was slightly higher than that of the control group, indicating favorable cell compatibility. Additionally, staining results showed healthy and well-stretched cells after 2−5 days of culture, consistent with the robust cell proliferation observed in the CCK-8 assay.

As depicted in Figure 7A, the sample was surgically implanted over the bone defect area. After 2 and 4 weeks of implantation, 3D reconstructed images illustrated the gradual regeneration of new bone tissue at the defect sites, accompanied by a noticeable reduction in the defect area. The most extensive regeneration occurred in the CaP/Ti/PCL/SF/PDA group by week 4, where the defects were nearly filled with new bone. Quantitative analysis using CT Analyzer software revealed a significant increase in bone volume to total volume (BV/TV) and bone mineral density (BMD) at the defect sites. At 4 weeks, there was no significant difference in

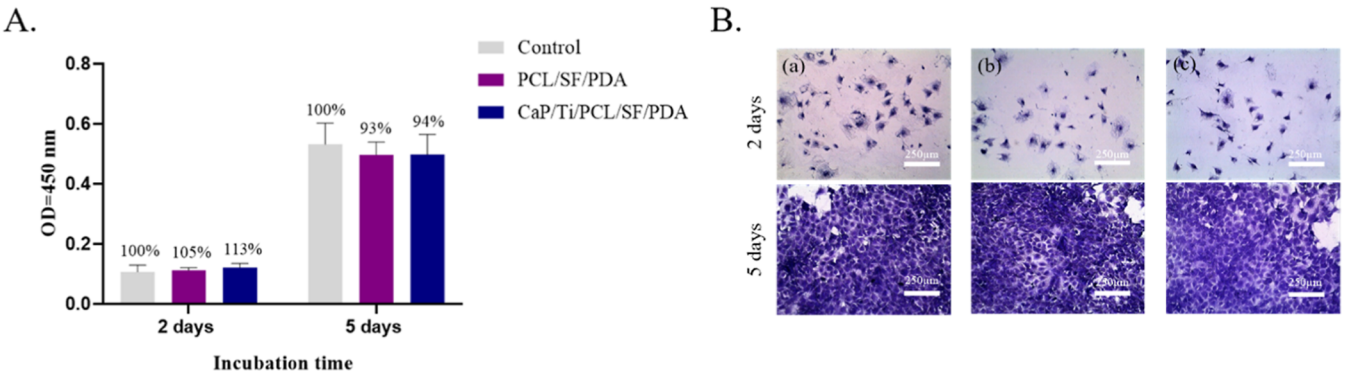

Figure 6. Cell proliferation and viability assessment. (A) MC3T3-E1 cell proliferation assessed via CCK-8 assay after 2 and 5 days of culture with the extracts. (B) Crystal violet staining of samples after 2 and 5 days: (a) control, (b) PCL/SF/PDA, and (c) CaP/Ti/PCL/SF/PDA.

https://doi.org/10.1021/acsomega.4c06731
ACS Omega 2025, 10, 14593−14601

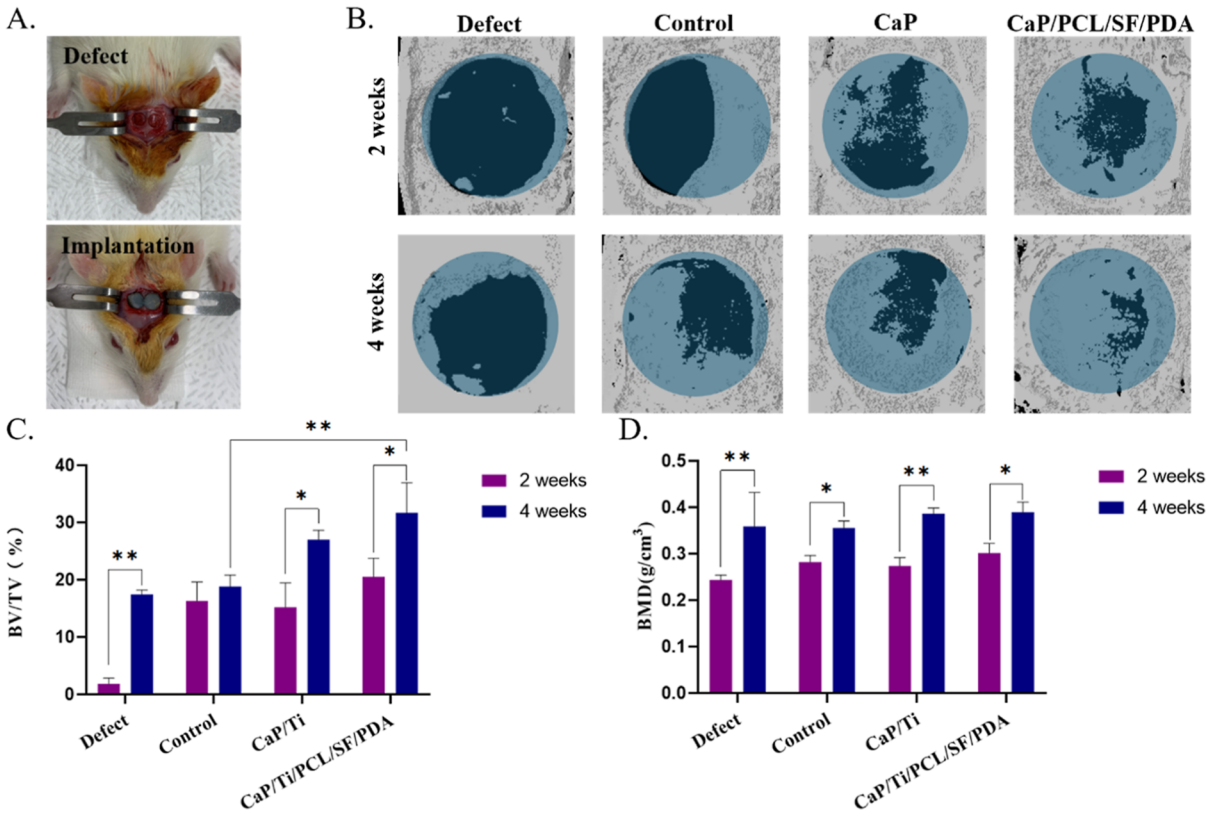

Figure 7. Evaluation of calvarial bone regeneration post-implantation. (A) Surgical photos depicting rat calvarial bone defect creation and Ti implantation. (B) Micro-CT reconstructed images showing calvarial defects after implantation for 2 and 4 weeks. (C) Quantitative analysis of bone tissue volume/total tissue volume (BV/TV) using CT Analyzer software. (D) Quantitative analysis of BMD using CT Analyzer software (#$p \geq 0.05$, * $p < 0.05$).

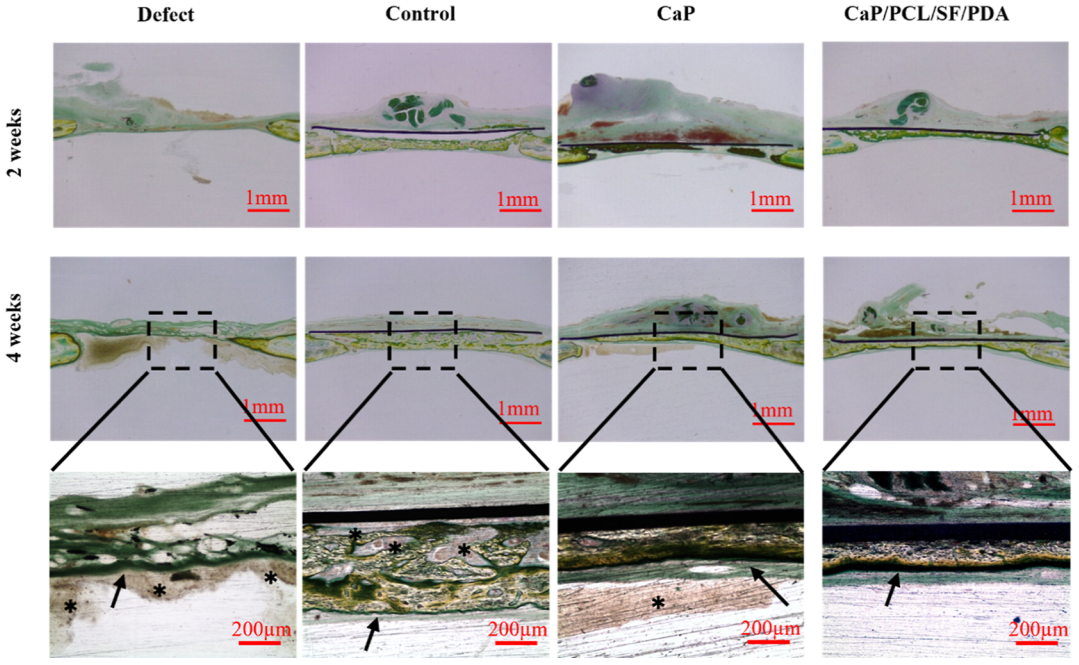

Figure 8. Bone regeneration at 2 and 4 weeks after surgery. Cross-sectional images (Villanueva bone staining, resin embedding) were obtained from the center points of each group of samples (arrow = new bone tissue, * = connective tissue).

BMD among the groups, indicating comparable levels of mineralization. However, the BV/TV ratio was markedly higher in the CaP/Ti/PCL/SF/PDA group (approximately 31.6%), significantly surpassing that of the other groups.

To further analyze bone regeneration, histological staining was conducted on the bone tissue samples, as shown in Figure 8. The staining results were highly consistent with the micro-CT analysis, revealing increased new bone formation at 4

https://doi.org/10.1021/acsomega.4c06731
ACS Omega 2025, 10, 14593−14601

weeks compared to that at 2 weeks. In the defect group, the area appeared filled with loose connective tissue. A noticeable gap was observed between the new bone layer and the Ti membrane in the control group, indicating the separation of the bone layer from the Ti sheet. In contrast, both the CaP and CaP/PCL/SF/PDA groups exhibited early-stage bone deposition along the CaP coating. New bone formation was evident along the Ti sheet, indicating strong bone-integration capability. Brown areas observed in the CaP group likely represented inflamed connective tissue, a phenomenon absent in the CaP/PCL/SF/PDA group.

DISCUSSION

Previous studies have successfully demonstrated the creation of microsized CaP deposits on Ti surfaces using an anodizing process combined with cyclic precalcification, significantly enhancing bone integration capabilities.[9] In this study, we utilized electrospray techniques to coat CaP/Ti substrates with biodegradable PCL drug-loaded nanoparticle coatings, aiming to effectively address inflammation through sustained release of anti-inflammatory drugs, thereby improving biocompatibility and accelerating the osseointegration process. XRD results in Figure 1B, line (a), reveal characteristic diffraction peaks of pure Ti, with the primary peak around 40°. Following electrochemical anodization and cyclic precalcification treatment, line (b) shows diffraction peaks corresponding to HA and OCP,[37] indicating the successful preparation of a CaP deposition layer on the Ti surface predominantly composed of HA and OCP phases. The Ti diffraction peak at approximately 40° was slightly attenuated due to the masking effect of the CaP deposition. Additionally, an increased peak around 38° suggests overlapping diffraction peaks from TiO_2 formed during the anodization process.[38] PCL drug-loaded nanoparticles were successfully deposited on the CaP/Ti surface via electrospraying (Figure 1A). Similar polymer-based drug delivery coatings have been developed in the past, utilizing methods such as spray coating, dip coating, and tape casting. However, challenges related to coating uniformity and drug loading efficiency have persisted.[23,39] The electrospraying technique facilitated uniform particle distribution with a controllable particle size of approximately 10.25 μm (Figure 1C), likely contributing to improved biocompatibility compared to traditional drug-loaded polymer coatings known for their heterogeneous distribution.[23,24] In the CaP/Ti/PCL/SF/PDA composite coating group, the introduction of PCL/SF/PDA did not markedly alter the crystal structure of the samples. However, the presence of the polymer coating led to a reduction in the intensity of certain diffraction peaks.

Although the PCL nanoparticle coatings were successfully prepared, they exhibited only weak van der Waals forces with the polymer and CAP/Ti, resulting in easy detachment from the surface. To address this issue, SF and PDA were introduced. In the FTIR results depicted in Figure 2, characteristic peaks at 3336.73 cm^{-1}, 3036.77 cm^{-1}, 2956.15 cm^{-1}, and 1498.08 cm^{-1} were identified as the stretching vibrations of −NH, −OH groups associated with the catechol structure, aromatic −CH, and the stretching of C═C in the benzene ring of DA, respectively, confirming the presence of DA. Upon self-polymerization in a weakly alkaline solution, these distinct peaks disappeared, with weaker peaks emerging in the 3500−2800 cm^{-1} range, corresponding to the stretching vibrations of free $-NH_2$ groups in PDA. The successful preparation of PDA through self-polymerization is evident.[40,41] In the CaP/Ti/PCL/SF/PDA group, peaks located at 3268.11 cm^{-1}, 1638.45 cm^{-1}, 1515.02 cm^{-1}, and 1236.38 cm^{-1} were attributed to SF.[42] Absorption peaks attributed to PCL were completely obscured under the SF/PDA gel, with no new peaks observed, indicating only physically meaningful coverage between them. Notably, the intensities of all peaks in the SF/PDA gel were significantly enhanced compared to those in PDA and SF, indicating a much higher hydrogen bonding content and thus better adhesion. A tape test was conducted to confirm the enhanced stability of the composite coating provided by the SF/PDA gel. The results demonstrated that only a minimal amount of PCL nanoparticles were forcibly removed before and after the experiment. This was in stark contrast to the pure PCL group, where almost all nanoparticles detached, indicating a significant improvement in stability. Such enhancement substantially increases the flexibility of clinical operations.

The degradation behaviors of the CaP/Ti/PCL/SF/PDA composite coatings are illustrated in Figure 4. The degradation rates of the SF/PDA gel differed from those of PCL, resulting in gradual degradation of the outer SF/PDA gel layer within 1 day. This slow degradation process gradually exposed the inner layer of PCL drug-loaded nanoparticles. The drug release profile within the first 24 h closely aligned with the degradation pattern of the coating, wherein the composite coating group exhibited a slower drug release rate compared to the pure PCL group. The initial encapsulation by the SF/PDA gel facilitated controlled early-stage drug release from the coating.

Cytotoxicity tests were conducted on MC3T3-E1 cells using extracts from each group of samples to assess the biocompatibility of the coating layer. The results demonstrated that cell viability in all sample groups was above 90% compared to the control group, indicating robust cell proliferation. Additionally, staining results showed that cells in all groups displayed healthy characteristics, with good elongation and expansion. These observations were consistent with CCK-8 results, indicating normal proliferation. No significant cytotoxicity was observed, confirming excellent biocompatibility.

2 and 4 weeks postimplantation, bone tissues were harvested for micro-CT and histological staining. 3D reconstruction images illustrated superior bone healing effects in the CaP/Ti/PCL/SF/PDA experimental group compared to other groups. The control group exhibited enhanced bone tissue regeneration along the Ti membrane direction, benefiting from the supportive effect of the Ti implant. In contrast, minimal new bone formation was observed in the defect group, localized only at the defect edges. The CaP/Ti group showed slightly improved bone healing compared to the control group, though this enhancement was less pronounced in the 3D reconstructed images. Quantitative analysis substantiated these findings, revealing a significant increase in BV/TV ratios in both the CaP/Ti and CaP/Ti/PCL/SF/PDA groups. This improvement is attributed to the presence of CaP deposits, enhancing the bone reconstruction environment of the implant and accelerating mineralization processes.[9,35,43] BMD results further indicated superior mineralization associated with CaP deposits. Histological staining corroborated these findings, showing loose connective tissue filling in the defect group and a modest increase in BV in the control group. However, extensive connective tissue infiltration into bone tissue was noted, with a clear separation from the Ti sheet, indicating weak surface osteoaffinity. This limited affinity is primarily due to initial osteogenesis occurring distally on the Ti implant

https://doi.org/10.1021/acsomega.4c06731
ACS Omega 2025, 10, 14593−14601

surface during early bone healing, with gradual mineralization extending from bone to the original Ti implant over several months.[44] In contrast, the bioactive surfaces of the CaP/Ti and CaP/Ti/PCL/SF/PDA groups exhibited initial contact osteogenesis on the implant surface.[35,44] Bone deposition along the Ti sheet was observed early postimplantation, underscoring the excellent bone integration capability of the CaP coating. Notably, inflammatory soft tissue invasion was observed in the defect, control, and CaP/Ti groups but was absent in the CaP/Ti/PCL/SF/PDA experimental group, which displayed the most favorable bone healing effect, nearly closing the defect after 4 weeks of repair. This effect is likely attributed to dexamethasone release, inhibiting pro-inflammatory factors,[12] reducing local inflammation, and fostering optimal conditions for osteoblast proliferation and differentiation.

CONCLUSION

In this study, we developed a drug-loaded polymer coating incorporating a CaP deposition layer to mitigate inflammation via controlled drug release and enhance coating stability, thereby improving the biocompatibility of Ti surfaces and accelerating osseointegration. Initially, a micrometer-scale CaP deposit was prepared on a Ti surface using an anodizing process combined with a cyclic precalcification method. Subsequently, electrospray technology was employed to apply a uniform layer of PCL drug-loaded nanoparticles. To address potential coating detachment issues, SF and PDA were introduced to form cohesive PCL/SF/PDA composite drug-loaded coatings. The incorporation of SF/PDA substantially enhanced the interaction between the polymer coating and the CaP/Ti substrate, thereby significantly improving stability. All materials exhibited favorable biocompatibility. In vivo experiments demonstrated that the CaP/Ti/PCL/SF/PDA samples effectively combined the bone affinity of CaP deposits with the anti-inflammatory properties of the PCL/SF/PDA drug-release coating, resulting in superior osseointegration. This study offers an effective surface modification strategy to enhance the performance of Ti implants. Future research will focus on quantitatively analyzing coating stability and long-term drug release behavior and elucidating specific anti-inflammatory and osteogenic mechanisms of dexamethasone.

AUTHOR INFORMATION

Corresponding Authors

Yu-Kyoung Kim − *Department of Dental Biomaterials, Institute of Biodegradable Materials, School of Dentistry, Jeonbuk National University, Jeon-Ju 54896, South Korea*; Email: yk0830@naver.com

Yong-Seok Jang − *Department of Dental Biomaterials, Institute of Biodegradable Materials, School of Dentistry, Jeonbuk National University, Jeon-Ju 54896, South Korea*; orcid.org/0000-0002-2757-232X; Email: yjang@jbnu.ac.kr

Min-Ho Lee − *Department of Dental Biomaterials, Institute of Biodegradable Materials, School of Dentistry, Jeonbuk National University, Jeon-Ju 54896, South Korea*; orcid.org/0000-0001-6142-4876; Email: mh@jbnu.ac.kr

Author

Hao An − *Department of Dental Biomaterials, Institute of Biodegradable Materials, School of Dentistry, Jeonbuk National University, Jeon-Ju 54896, South Korea*

Complete contact information is available at: https://pubs.acs.org/10.1021/acsomega.4c06731

Author Contributions

Conceptualization, H.A., Y.-K.K., M.-H.L., and Y.-S.J.; performed experiments, H.A.; analyzed data, H.A.; writing—original draft preparation, H.A.; writing—review and editing, H.A, Y.-K.K., M.-H.L., and Y.-S.J. (all authors had the final input); visualization, H.A.; supervision, Y.-K.K., M.-H.L., and Y.-S.J.; project administration, Y.-K.K., M.-H.L., and Y.-S.J.; funding acquisition, Y.-S.J. and M.-H.L. All authors have read and agreed to the published version of the manuscript.

Funding

The animal study protocol was approved by the Institutional Review Board of Jeonbuk National University, Laboratory Animal Center, Jeonju-si, South Korea (approval number: NON2023-206-001, approval date: 13 December 2023).

Notes

The authors declare no competing financial interest.

The authors declare that they have no competing financial interests or personal relationships that may have influenced the work reported in this study.

ACKNOWLEDGMENTS

This research was supported by the "National Research Foundation of Korea (NRF) grant funded by the Korea government (MSIT) (NRF- 2021R1A2C2005466 and NRF-2021R1A2C1008740)". This study has reconstructed the data of H.A.'s master dissertation submitted in 2023 (Title: Polycaprolactone/silk fibroin/PDA composite coating formed on Ti by electrospray technology).

ABBREVIATIONS

CaP, calcium phosphate; PCL, polycaprolactone; SF, silk fibroin; PDA, polydopamine

REFERENCES

(1) Sarraf, M.; Ghomi, E. R.; Alipour, S.; Ramakrishna, S.; Sukiman, N. L. A state-of-the-art review of the fabrication and characteristics of titanium and its alloys for biomedical applications. *Bio-Des. Manuf.* **2022**, *5* (2), 371−395.

(2) Li, Y.; Yang, C.; Zhao, H.; Qu, S.; Li, X.; Li, Y. New Developments of Ti-Based Alloys for Biomedical Applications. *Materials* **2014**, *7* (3), 1709−1800.

(3) Sidhu, S. S.; Gepreel, M. A. H.; Bahraminasab, M. Advances in titanium bio-implants: Alloy design, surface engineering and manufacturing processes. *J. Mater. Res.* **2022**, *37* (16), 2487−2490.

(4) Kligman, S.; Ren, Z.; Chung, C. H.; Perillo, M. A.; Chang, Y. C.; Koo, H.; Zheng, Z.; Li, C. The Impact of Dental Implant Surface Modifications on Osseointegration and Biofilm Formation. *J. Clin. Med.* **2021**, *10* (8), 1641.

(5) Hoque, M. E.; Showva, N. N.; Ahmed, M.; Rashid, A. B.; Sadique, S. E.; El-Bialy, T.; Xu, H. Titanium and titanium alloys in dentistry: current trends, recent developments, and future prospects. *Heliyon* **2022**, *8* (11), No. e11300.

(6) Xue, N.; Ding, X.; Huang, R.; Jiang, R.; Huang, H.; Pan, X.; Min, W.; Chen, J.; Duan, J. A.; Liu, P.; et al. Bone Tissue Engineering in the Treatment of Bone Defects. *Pharmaceuticals* **2022**, *15* (7), 879.

(7) Hu, X. X.; Shen, H.; Shuai, K. G.; Zhang, E. W.; Bai, Y. J.; Cheng, Y.; Xiong, X. L.; Wang, S. G.; Fang, J.; Wei, S. C. Surface bioactivity modification of titanium by CO_2 plasma treatment and induction of hydroxyapatite: In vitro and in vivo studies. *Appl. Surf. Sci.* **2011**, *257* (6), 1813−1823.

(8) Gu, Y. X.; Du, J.; Zhao, J. M.; Si, M. S.; Mo, J. J.; Lai, H. C. Characterization and preosteoblastic behavior of hydroxyapatite-deposited nanotube surface of titanium prepared by anodization

coupled with alternative immersion method. *J. Biomed. Mater. Res. B Appl. Biomater.* **2012**, *100B* (8), 2122.
(9) Nguyen, T. D.; Moon, S. H.; Oh, T. J.; Park, I. S.; Lee, M. H.; Bae, T. S. The effect of APH treatment on surface bonding and osseointegration of Ti-6Al-7Nb implants: an in vitro and in vivo study. *J. Biomed. Mater. Res. B Appl. Biomater.* **2015**, *103* (3), 641−648.
(10) Birajdar, M. S.; Joo, H.; Koh, W. G.; Park, H. Natural bio-based monomers for biomedical applications: a review. *Biomater. Res.* **2021**, *25* (1), 8.
(11) Ogay, V.; Mun, E. A.; Kudaibergen, G.; Baidarbekov, M.; Kassymbek, K.; Zharkinbekov, Z.; Saparov, A. Progress and Prospects of Polymer-Based Drug Delivery Systems for Bone Tissue Regeneration. *Polymers* **2020**, *12* (12), 2881.
(12) Cato, A. C.; Wade, E. Molecular mechanisms of anti-inflammatory action of glucocorticoids. *Bioessays* **1996**, *18* (5), 371−378.
(13) Bhadran, A.; Shah, T.; Babanyinah, G. K.; Polara, H.; Taslimy, S.; Biewer, M. C.; Stefan, M. C. Recent Advances in Polycaprolactones for Anticancer Drug Delivery. *Pharmaceutics* **2023**, *15* (7), 1977.
(14) Shen, J.; Yuan, W.; Badv, M.; Moshaverinia, A.; Weiss, P. S. Modified Poly(epsilon-caprolactone) with Tunable Degradability and Improved Biofunctionality for Regenerative Medicine. *ACS Mater. Au* **2023**, *3* (5), 540−547.
(15) Fernández, J.; Etxeberria, A.; Sarasua, J.-R. In vitro degradation studies and mechanical behavior of poly(ε-caprolactone-co-δ-valerolactone) and poly(ε-caprolactone-co-L-lactide) with random and semi-alternating chain microstructures. *Eur. Polym. J.* **2015**, *71*, 585−595.
(16) Jaworek, A.; Sobczyk, A. T.; Krupa, A. Electrospray application to powder production and surface coating. *J. Aerosol Sci.* **2018**, *125*, 57−92.
(17) Castillo, J. L.; Martin, S.; Rodriguez-Perez, D.; Higuera, F. J.; Garcia-Ybarra, P. L. Nanostructured porous coatings via electrospray atomization and deposition of nanoparticle suspensions. *J. Aerosol Sci.* **2018**, *125*, 148−163.
(18) Kumbar, S. G.; Bhattacharyya, S.; Sethuraman, S.; Laurencin, C. T. A preliminary report on a novel electrospray technique for nanoparticle based biomedical implants coating: precision electrospraying. *J. Biomed. Mater. Res. B Appl. Biomater.* **2007**, *81B* (1), 91−103.
(19) Sridhar, R.; Ramakrishna, S. Electrosprayed nanoparticles for drug delivery and pharmaceutical applications. *Biomatter* **2013**, *3* (3), No. e24281.
(20) Boda, S. K.; Li, X.; Xie, J. Electrospraying an enabling technology for pharmaceutical and biomedical applications: A review. *J. Aerosol Sci.* **2018**, *125*, 164−181.
(21) Bonadies, I.; Maglione, L.; Ambrogi, V.; Paccez, J. D.; Zerbini, L. F.; e Silva, L. F. R.; Picanco, N. S.; Tadei, W. P.; Grafova, I.; Grafov, A.; et al. Electrospun core/shell nanofibers as designed devices for efficient Artemisinin delivery. *Eur. Polym. J.* **2017**, *89*, 211−220.
(22) Patra, J. K.; Das, G.; Fraceto, L. F.; Campos, E. V. R.; Rodriguez-Torres, M. D. P.; Acosta-Torres, L. S.; Diaz-Torres, L. A.; Grillo, R.; Swamy, M. K.; Sharma, S.; et al. Nano based drug delivery systems: recent developments and future prospects. *J. Nanobiotechnol.* **2018**, *16* (1), 71.
(23) Butt, M. A. Thin-Film Coating Methods: A Successful Marriage of High-Quality and Cost-Effectiveness-A Brief Exploration. *Coatings* **2022**, *12* (8), 1115.
(24) Zhang, Z.; Feng, S. S. The drug encapsulation efficiency, in vitro drug release, cellular uptake and cytotoxicity of paclitaxel-loaded poly(lactide)-tocopheryl polyethylene glycol succinate nanoparticles. *Biomaterials* **2006**, *27* (21), 4025−4033.
(25) Chen, S. Y.; Liu, S.; Zhang, L. L.; Han, Q.; Liu, H. Q.; Shen, J. H.; Li, G. C.; Zhang, L. Z.; Yang, Y. M. Construction of injectable silk fibroin/polydopamine hydrogel for treatment of spinal cord injury. *Chem. Eng. J.* **2020**, *399*, 125795.
(26) Liu, M. Y.; Zeng, G. J.; Wang, K.; Wan, Q.; Tao, L.; Zhang, X. Y.; Wei, Y. Recent developments in polydopamine: an emerging soft matter for surface modification and biomedical applications. *Nanoscale* **2016**, *8* (38), 16819−16840.
(27) Sun, W. Z.; Gregory, D. A.; Tomeh, M. A.; Zhao, X. B. Silk Fibroin as a Functional Biomaterial for Tissue Engineering. *Int. J. Mol. Sci.* **2021**, *22* (3), 1499.
(28) Qi, Y.; Wang, H.; Wei, K.; Yang, Y.; Zheng, R. Y.; Kim, I. S.; Zhang, K. Q. A Review of Structure Construction of Silk Fibroin Biomaterials from Single Structures to Multi-Level Structures. *Int. J. Mol. Sci.* **2017**, *18* (3), 237.
(29) Zhang, C.; Xiang, L.; Zhang, J.; Liu, C.; Wang, Z.; Zeng, H.; Xu, Z. K. Revisiting the adhesion mechanism of mussel-inspired chemistry. *Chem. Sci.* **2022**, *13* (6), 1698−1705.
(30) Xiong, X.; Liu, Y. M.; Shi, F.; Zhang, G. W.; Weng, J.; Qu, S. X. Enhanced Adhesion of Mussel-inspired Adhesive through Manipulating Contents of Dopamine Methacrylamide and Molecular Weight of Polymer. *JBE* **2018**, *15* (3), 461−470.
(31) Ahn, B. K. Perspectives on Mussel-Inspired Wet Adhesion. *J. Am. Chem. Soc.* **2017**, *139* (30), 10166−10171.
(32) Xiao, Z. B.; Liu, H. Q.; Zhao, Q. X.; Niu, Y. W.; Zhao, D. Silk fibroin/polydopamine modified nanocapsules for high-performance adhesion. *Colloids Surf., A* **2022**, *646*, 128951.
(33) Kim, S. Y.; Kim, Y. K.; Park, I. S.; Jin, G. C.; Bae, T. S.; Lee, M. H. Effect of alkali and heat treatments for bioactivity of TiO_2 nanotubes. *Appl. Surf. Sci.* **2014**, *321*, 412−419.
(34) Nguyen, T. T.; Jang, Y. S.; Kim, Y. K.; Kim, S. Y.; Lee, M. H.; Bae, T. S. Osteogenesis-Related Gene Expression and Guided Bone Regeneration of a Strontium-Doped Calcium-Phosphate-Coated Titanium Mesh. *ACS Biomater. Sci. Eng.* **2019**, *5* (12), 6715−6724.
(35) Nguyen, P. M. H.; Won, D. H.; Kim, B. S.; Jang, Y. S.; Nguyen, T. D. T.; Lee, M. H.; Bae, T. S. The effect of two-step surface modification for Ti-Ta-Mo-Zr alloys on bone regeneration: An evaluation using calvarial defect on rat model. *Appl. Surf. Sci.* **2018**, *442*, 630−639.
(36) Park, J. E.; Kim, Y. K.; Kim, S. Y.; Choi, J. B.; Bae, T. S.; Jang, Y. S.; Lee, M. H. Biocompatibility and Antibacterial Effect of Ginger Fraction Loaded PLGA Microspheres Fabricated by Coaxial Electrospray. *Materials* **2023**, *16* (5), 1885.
(37) Oh, E. J.; Nguyen, T. D.; Lee, S. Y.; Jeon, Y. M.; Bae, T. S.; Kim, J. G. Enhanced compatibility and initial stability of Ti6Al4V alloy orthodontic miniscrews subjected to anodization, cyclic precalcification, and heat treatment. *Korean J. Orthod.* **2014**, *44* (5), 246−253.
(38) Yurdakal, S.; Augugliaro, V.; Loddo, V.; Palmisano, G.; Palmisano, L. Enhancing selectivity in photocatalytic formation of p-anisaldehyde in aqueous suspension under solar light irradiation via TiO_2 N-doping. *New J. Chem.* **2012**, *36* (9), 1762−1768.
(39) Alfatama, M.; Shahzad, Y.; Choukaife, H. Recent advances of electrospray technique for multiparticulate preparation: Drug delivery applications. *Adv. Colloid Interface Sci.* **2024**, *325*, 103098.
(40) Lee, H.; Dellatore, S. M.; Miller, W. M.; Messersmith, P. B. Mussel-inspired surface chemistry for multifunctional coatings. *Science* **2007**, *318* (5849), 426−430.
(41) Lagutschenkov, A.; Langer, J.; Berden, G.; Oomens, J.; Dopfer, O. Infrared spectra of protonated neurotransmitters: dopamine. *Phys. Chem. Chem. Phys.* **2011**, *13* (7), 2815−2823.
(42) Dong, Y.; Dong, P.; Huang, D.; Mei, L.; Xia, Y.; Wang, Z.; Pan, X.; Li, G.; Wu, C. Fabrication and characterization of silk fibroin-coated liposomes for ocular drug delivery. *Eur. J. Pharm. Biopharm.* **2015**, *91*, 82−90.
(43) Barrere, F.; van der Valk, C. M.; Meijer, G.; Dalmeijer, R. A.; de Groot, K.; Layrolle, P. Osteointegration of biomimetic apatite coating applied onto dense and porous metal implants in femurs of goats. *J. Biomed. Mater. Res. B Appl. Biomater.* **2003**, *67B* (1), 655−665.
(44) Masuda, T.; Yliheikkila, P. K.; Felton, D. A.; Cooper, L. F. Generalizations regarding the process and phenomenon of osseointegration. Part I. In vivo studies. *Int. J. Oral Maxillofac. Implants* **1998**, *13* (1), 17−29.

https://doi.org/10.1021/acsomega.4c06731
ACS Omega 2025, 10, 14593−14601